# Supporting information for:

## Rational Design of $MoS_2$ Catalysts: Tuning the Structure and Activity *via* Transition Metal Doping

Charlie Tsai,[†,‡] Karen Chan,[†,‡] Jens K. Nørskov,[†,‡] and Frank Abild-Pedersen[*,‡]

*Department of Chemical Engineering, Stanford University, Stanford, California 94305, USA, and SUNCAT Center for Interface Science and Catalysis, SLAC National Accelerator Laboratory, Menlo Park, California 94025, USA*

E-mail: abild@slac.stanford.edu

# 1 Calculation details

All results were calculated using plane-wave density functional theory (DFT) employing ultrasoft-pseudopotentials. The QUANTUM ESPRESSO code[S1] and the BEEF-vdW exchange-correlation functional[S2–S5] were used for all calculations. The plane-wave cutoff and density cutoff were 500 eV and 5000 eV respectively, where convergence testing on $MoS_2$ had been done previously.[S6] The bulk lattice constants for $MoS_2$ were determined to be $a = 3.19$ Å and $c = 13.05$ Å, in reasonable agreement with the experimentally determined value of $a = 3.16$ Å and $c = 12.29$ Å.[S7–S9] The small discrepancy in the $c$ parameter should have no significant effect on our results, as we only considered single layers in this study. An infinite stripe model described previously[S10–S13] was used to investigate the S-edge (shown in Figure 1A in the main text). In the infinite stripe, both the Mo-edge and the S-edge are exposed. When studying the S-edge, the exact configuration of the Mo-edge is unimportant so long as it is kept constant.

Two unit cell sizes were used for the infinite stripe (Figure 1A of the main text): the larger unit cell was used to describe coverages of $\theta_H = 0.25$ and 0.75 ML and the smaller unit cell was used to describe coverages of $\theta_H = 0$, 0.5, and 1.0 ML. Using periodic boundary conditions in all directions, the $MoS_2$ stripes were separated by at least 9 Å of vacuum in the $y$-direction and 11 Å in the $z$-direction. The Brillouin zone was sampled by a Monkhorst-Pack $2\times1\times1$ and $4\times1\times1$ k-point grid for the large and small unit cells respectively.[S14] The structures were relaxed until the total forces were less than 0.05 eV/Å. Spin-polarized calculations were performed for Fe and Mn-doped $MoS_2$, since they exhibited structural and energetic differences when including spin-polarization and without spin-polarization.

[*]To whom correspondence should be addressed

[†]Department of Chemical Engineering, Stanford University, Stanford, California 94305, USA

[‡]SUNCAT Center for Interface Science and Catalysis, SLAC National Accelerator Laboratory, Menlo Park, California 94025, USA

# 2 Adsorption energies

Differential adsorption energies are defined in the same way as in previous studies for H[S6,S12,S15] and S.[S16–S18] The hydrogen adsorption energy was defined as

$$\Delta E_{\mathrm{H}} = E(\mathrm{stripe}+\mathrm{H}) - E(\mathrm{stripe}) - \frac{1}{2}E(\mathrm{H_2}) \tag{1}$$

and the S adsorption energy was calculated as

$$\Delta E_{\mathrm{S}} = E(\mathrm{stripe}) + E(\mathrm{H_2}) - E(\mathrm{H_2S}) - E(\mathrm{stripe}-\mathrm{S}) \tag{2}$$

where the desorption energy is $-\Delta E_{\mathrm{S}}$. The adsorption free energies $\Delta G$ were then calculated as

$$\Delta G = \Delta E + \Delta E_{\mathrm{ZPE}} - T\Delta S \tag{3}$$

where $\Delta E_{\mathrm{ZPE}}$ is the difference in zero point energy, $T$ is the temperature and $\Delta S$ is the difference in entropy relative to the gas phase standard state (300 K, 1 bar) for $H_2$. For $H_2S$ a pressure of $10^{-6}$ bar was chosen instead, following standard corrosion resistance.[S19,S20] The $\Delta E_{\mathrm{ZPE}}$ and $\Delta S$ are determined through the vibrational frequencies of the adsorbed hydrogen using a normal mode analysis.[S21]

# 3 Stable edge structure determination

The specific edge structure (i.e., the S and H coverage) is known to be highly sensitive to the synthesis or reaction conditions. We have calculated the Stable edge structures under hydrogen evolution reaction (HER) conditions according to a previously established method.[S22,S23] We summarize the approach here. Using the calculated energies of the infinite stripes with each possible configuration, the free energy of the edge $\gamma$ was then determined by $\gamma = \left[G_{\mathrm{stripe}} - \sum_i N_i\mu_i\right]/2L$, where the sum is over all $i$ constituents of the stripe and $L$ is the length of the unit cell. It is often more convenient to define the edge free energy in terms of a reference edge. For each doped edge, we have chosen their respective edges at coverages of $\theta_{\mathrm{S}} = 0$ ML and $\theta_{\mathrm{H}} = 0$ ML as the reference. $\gamma$ is then

$$\gamma = \frac{1}{2L}\left(G_{\mathrm{stripe}} - N_{\mathrm{S}}\mu_{\mathrm{S}} - N_{\mathrm{H}}\mu_{\mathrm{H}}\right) - \frac{G^{\mathrm{ref}}_{\mathrm{stripe}}}{2L} \tag{4}$$

where $G_{\mathrm{stripe}}$ is the free energy of the infinite stripe, and $G^{\mathrm{ref}}_{\mathrm{stripe}}$ is the reference stripe. Under reducing conditions for HER, the equilibrium reactions

$$2\left(\mathrm{H^+ + e^-}\right) + \mathrm{S}(^*) \rightleftharpoons \mathrm{H_2S} + (^*) \tag{5}$$

and

$$\mathrm{H^+ + e^-} \rightleftharpoons \mathrm{H} \tag{6}$$

determine the chemical potentials. Here, $(^*)$ represents a S vacancy on the edge. Using the computational hydrogen electrode (CHE),[S24,S25] the chemical potentials can be written in terms of the applied bias, $U_{\mathrm{RHE}}$ (defined relative to the reversible hydrogen electrode), as

$$\mu_{\mathrm{H}} = \frac{1}{2}\mu_{\mathrm{H_2}} - eU_{\mathrm{RHE}} \tag{7}$$

and

$$\mu_S = \mu_{H_2S} - 2\mu_H = \mu_{H_2S} - 2\left(\frac{1}{2}\mu_{H_2} - eU_{RHE}\right) \quad (8)$$

where we have chosen a pressure for $H_2S$ of $10^{-6}$ bar, following standard corrosion resistance.[S19,S20]

Our approach then is to take the most thermodynamically stable edge configuration at $U_{RHE} = 0$ V (since we are interested in the low over-potential range in $U_{RHE} < 0$ V) according to their edge free energies $\gamma$, and then assume that the steady state H coverage is where $H_2$ evolution is more exergonic than the desorption of $(^*)$SH as $H_2S$ or further H adsorption. In reality, the desorption of SH as $H_2S$ should be kinetically limited by hydrogen evolution at the S sites, since the pressure of $H_2S$ is negligible under operating conditions, yet $MoS_2$ catalysts have been found to be remarkably stable.[S13,S26,S27] However, since adsorption energies are known to scale with activation energies, we use the thermodynamic analysis as a first approximation.[S28,S29] A detailed kinetic analysis will be considered in future studies.

# 4 The effect of edge reconstruction on the adsorption energies

Generally, there are geometric rearrangements on the edge when hydrogen is adsorbed onto sulfur. These can range from small shifts in the positions of the sulfur atoms (Fig. S1a), to the breaking of a S-S dimer bond (Fig. S1b). The energetic contribution from the rearrangement can range from approximately $+0.1$ eV to $+1.0$ eV. This phenomena has been discussed in more detail previously.[S6,S22,S30] Examples of each type of edge rearrangement are shown below.

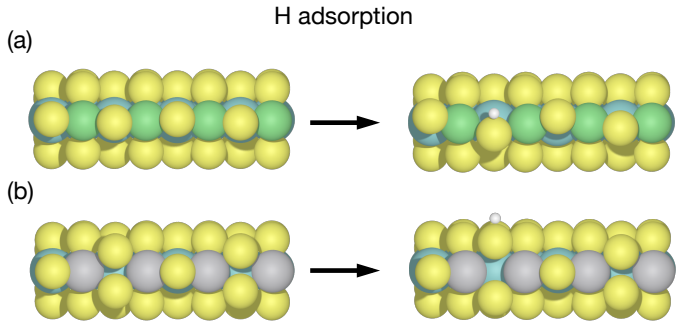


Figure S1: (a) edge reconstruction due to hydrogen adsorption onto a single sulfur atom, resulting in rearrangements of the sulfur atoms; (b) edge reconstruction due to S−H bond formation, which breaks the S−S dimer bond.

# 5 Summary of stable edge structures

In Table S1 we summarize the Stable edge structures determined. The hydrogen coverages were determined as a fraction of the available binding sites. For the structures with S vacancies, we counted each vacancy as a site. Generally, hydrogen adsorption is more exergonic at the edge-most S sites, even for structures with S vacancies. As discussed in the main text, the reason for this is that the structures with lower S coverages are also weaker at binding S to the edge, which in turn results in stronger binding of the H atom to the S atom rather than to the edge-most metal. We have focused on the edge-most S atoms and edge-most metal dopant atoms in this study and have not considered the effect of doping into the basal plane.

Table S1: Stable structures for each doped edge. The $\Delta G_{\mathrm{H}}^{\mathrm{eq}}$ are determined at the final adsorbed hydrogen for the structures shown.

| Dopant | Structure | $\theta_{\mathrm{S}}$ (ML) | $\theta_{\mathrm{H}}$ (ML) | $\Delta G_{\mathrm{H}}^{\mathrm{eq}}$ (eV) |
|---|---|---|---|---|
| V | 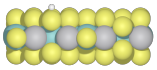 | 0.75 | 0.25 | 0.08 |
| Nb | 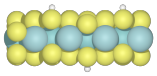 | 1.0 | 0.75 | 0.21 |
| Ta | 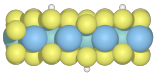 | 1.0 | 0.75 | 0.06 |
| Cr | 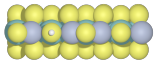 | 0.5 | 0.25 | 0.21 |
| Mo | 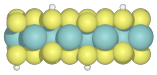 | 1.0 | 1.0 | −0.45 |
| W | 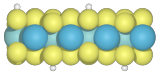 | 1.0 | 1.0 | −0.70 |
| Mn | 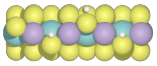 | 0.5 | 0.75 | 0.05 |
| Re | 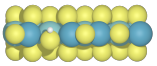 | 0.5 | 0.25 | 0.40 |
| Fe | 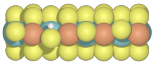 | 0.5 | 0.25 | 0.04 |
| Ru | 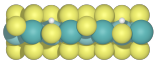 | 0.5 | 0.50 | 0.01 |
| Os | 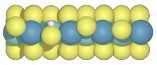 | 0.5 | 0.25 | 0.23 |
| Co | 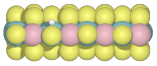 | 0.5 | 0.25 | 0.01 |
| Rh | 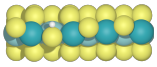 | 0.5 | 0.25 | 0.01 |
| Ir | 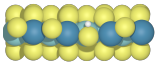 | 0.5 | 0.25 | 0.27 |
| Ni | 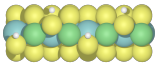 | 0.5 | 1.0 | −0.15 |
| Pd | 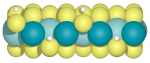 | 0.5 | 1.0 | −0.57 |
| Pt | 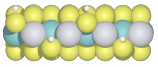 | 0.5 | 1.0 | −0.37 |
| Cu | 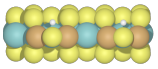 | 0.25 | 0.50 | −0.55 |
| Ag | 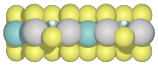 | 0.25 | 0.50 | −1.02 |
| Au | 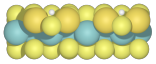 | 0.25 | 0.50 | −0.60 |

## References


(S1) Giannozzi, P.; Baroni, S.; Bonini, N.; Calandra, M.; Car, R.; Cavazzoni, C.; Ceresoli, D.; Chiarotti, G. L.; Cococcioni, M.; Dabo, I.; Dal Corso, A.; de Gironcoli, S.; Fabris, S.; Fratesi, G.; Gebauer, R.; Gerstmann, U.; Gougoussis, C.; Kokalj, A.; Lazzeri, M.; Martin-Samos, L.; Marzari, N.; Mauri, F.; Mazzarello, R.; Paolini, S.; Pasquarello, A.; Paulatto, L.; Sbraccia, C.; Scandolo, S.; Sclauzero, G.; Seitsonen, A. P.; Smogunov, A.; Umari, P.; Wentzcovitch, R. M. *J. Phys.: Condens. Matter* **2009**, *21*, 395502.

(S2) Wellendorff, J.; Lundgaard, K. T.; Møgelhøj, A.; Petzold, V.; Landis, D. D.; Nørskov, J. K.; Bligaard, T.; Jacobsen, K. W. *Phys. Rev. B* **2012**, *85*, 235149.

(S3) Dion, M.; Rydberg, H.; Schröder, E.; Langreth, D. C.; Lundqvist, B. I. *Phys. Rev. Lett.* **2004**, *92*, 246401.

(S4) Thonhauser, T.; Cooper, V. R.; Li, S.; Puzder, A.; Hyldgaard, P.; Langreth, D. C. *Phys. Rev. B* **2007**, *76*, 125112.

(S5) Román-Péréz, G.; Soler, J. M. *Phys. Rev. Lett.* **2009**, *103*, 096102.

(S6) Tsai, C.; Abild-Pedersen, F.; Nørskov, J. K. *Nano Lett.* **2014**, *14*, 1381–1387.

(S7) Raybaud, P.; Hafner, J.; Kresse, G.; Kasztelan, S.; Toulhoat, H. *J. Catal.* **2000**, *190*, 128–143.

(S8) Böker, T.; Severin, R.; Müller, A.; Janowitz, C.; Manzke, R.; Voß, D.; Krüger, P.; Mazur, A.; Pollmann, J. *Phys. Rev. B* **2001**, *64*, 235305.

(S9) Jellinek, F.; Brauer, G.; Müller, H. *Nature* **1960**, *185*, 376–377.

(S10) Byskov, L. S.; Nørskov, J. K.; Clausen, B. S.; Topsøe, H. *J. Catal.* **1999**, *187*, 109–122.

(S11) Bollinger, M. V.; Lauritsen, J. V.; Jacobsen, K. W.; Nørskov, J. K.; Helveg, S.; Besenbacher, F. *Phys. Rev. Lett.* **2001**, *87*, 196803.

(S12) Bollinger, M. V.; Jacobsen, K. W.; Nørskov, J. K. *Phys. Rev. B* **2003**, *67*, 085410.

(S13) Hinnemann, B.; Moses, P. G.; Bonde, J. L.; Jørgensen, K. P.; Nielsen, J. H.; Horch, S.; Chorkendorff, I.; Nørskov, J. K. *J. Am. Chem. Soc.* **2005**, *127*, 5308–5309.

(S14) Monkhorst, H. J.; Pack, J. D. *Phys. Rev. B* **1976**, *13*, 5188–5192.

(S15) Hinnemann, B.; Nørskov, J. K.; Topsøe, H. *J. Phys. Chem. B* **2005**, *109*, 2245–2253.

(S16) Fernández, E. M.; Moses, P. G.; Toftelund, A.; Hansen, H. A.; Martínez, J. I.; Abild-Pedersen, F.; Kleis, J.; Hinnemann, B.; Rossmeisl, J.; Bligaard, T.; Nørskov, J. K. *Angew. Chem. Int. Ed.* **2008**, *47*, 4683–4686.

(S17) Moses, P. G.; Hinnemann, B.; Topsøe, H.; Nørskov, J. K. *J. Catal.* **2007**, *248*, 188–203.

(S18) Moses, P. G.; Hinnemann, B.; Topsøe, H.; Nørskov, J. K. *J. Catal.* **2009**, *268*, 201–208.

(S19) Pourbaix, M. *Atlas D'equilibres Electrochimiques*; Gauthier-Villars: Paris, 1963.

(S20) Hansen, H. A.; Rossmeisl, J.; Nørskov, J. K. *Phys. Chem. Chem. Phys.* **2008**, *10*, 3722–3730.

(S21) Skúlason, E.; Tripkovic, V.; Björketun, M. E.; Gudmundsdóttir, S.; Karlberg, G. S.; Rossmeisl, J.; Bligaard, T.; Jónsson, H.; Nørskov, J. K. *J. Phys. Chem. C* **2010**, *114*, 18182–18197.

(S22) Tsai, C.; Chan, K.; Abild-Pedersen, F.; Nørskov, J. K. *Phys. Chem. Chem. Phys.* **2014**, 13156–13164.

(S23) Chan, K.; Tsai, C.; Hansen, H. A.; Nørskov, J. K. *ChemCatChem* **2014**,

(S24) Nørskov, J. K.; Bligaard, T.; Logadóttir, Á.; Kitchin, J. R.; Chen, J. G.; Pandelov, S.; Stimming, U. *J. Electrochem. Soc.* **2005**, *152*, J23–J26.

(S25) Peterson, A. A.; Abild-Pedersen, F.; Studt, F.; Rossmeisl, J.; Nørskov, J. K. *Energy Environ. Sci.* **2010**, *3*, 1311.

(S26) Jaramillo, T. F.; Jørgensen, K. P.; Bonde, J. L.; Nielsen, J. H.; Horch, S.; Chorkendorff, I. *Science* **2007**, *317*, 100–102.

(S27) Chen, Z.; Cummins, D.; Reinecke, B. N.; Clark, E.; Sunkara, M. K.; Jaramillo, T. F. *Nano Lett.* **2011**, *11*, 4168–4175.

(S28) Logadóttir, Á.; Rod, T. H.; Nørskov, J. K.; Hammer, B.; Dahl, S.; Jacobsen, C. *J. Catal.* **2001**, *197*, 229–231.

(S29) Bligaard, T.; Nørskov, J. K.; Dahl, S.; Matthiesen, J.; Christensen, C. H.; Sehested, J. *J. Catal.* **2004**, *224*, 206–217.

(S30) Byskov, L. S.; Bollinger, M. V.; Nørskov, J. K.; Clausen, B. S.; Topsøe, H. *J. Mol. Catal. A-Chem.* **2000**, *163*, 117–122.